PROCEEDINGS OF SCIENCE

CPV in beauty decays with LHCb

Frank Meier[*†]
Technische Universitaet Dortmund (DE)
E-mail: frank.meier@tu-dortmund.de

During 2011 and 2012, *pp* collision data corresponding to integrated luminosities of $1\,\mathrm{fb}^{-1}$ at a centre-of-mass energy of 7 TeV and $2\,\mathrm{fb}^{-1}$ at 8 TeV have been collected with the LHCb detector. This dataset has allowed LHCb to measure with unprecedented precision observables relating to the CKM unitary triangles. In these proceedings I describe measurements sensitive to γ, the least well constrained unitary triangle angle.

Fourth Annual Large Hadron Collider Physics
13-18 June 2016
Lund, Sweden

[*] Speaker.
[†] On behalf of the LHCb collaboration.

1. Introduction

In the Standard Model of particle physics (SM) the weak force is maximally violating *CP* conservation. A single irreducible phase in the Cabibbo-Kobayashi-Maskawa (CKM) matrix [1, 2] describes *CP* violation in the quark-mixing sector. The unitary CKM matrix relates the mass eigenstates with the eigenstates to the weak force of the three generations of down-type quarks. Its unitarity results in certain conditions, which can be expressed as closed triangles in the complex plane. The triangle that is usually referred to as the CKM triangle fulfils the condition

$$V_{ud}V_{ub}^* + V_{cd}V_{cb}^* + V_{td}V_{tb}^* = 0\,.$$

Precision measurements of the side lengths and angles of this triangle provide insight into the nature of *CP* violation. The least well known angle is $\gamma \equiv \arg[-(V_{ud}V_{ub}^*)/(V_{cd}V_{cb}^*)]$. This angle is unique in that it can be determined from tree-level only processes. Comparisons between direct measurements of γ and constraints coming from global fits, which include loop diagrams as well, offer a good opportunity to test the SM. To achieve this goal it is mandatory to improve the precision on tree-level measurements of γ. I present here recent measurements of γ using the full Run I data sample corresponding to an integrated luminosity of $3\,\mathrm{fb}^{-1}$ of *pp* collisions.

2. LHCb detector

The LHCb detector [3, 4] is a single-arm forward spectrometer covering the pseudorapidity range $2 < \eta < 5$, designed for the study of particles containing *b*- or *c*-quarks. The detector includes a high-precision tracking system consisting of a silicon-strip vertex detector surrounding the *pp* interaction region, a large-area silicon-strip detector located upstream of a dipole magnet, and three stations of silicon-strip detectors and straw drift tubes placed downstream of the magnet. Depending on the detector response two different type of $K^0_\mathrm{S} \to \pi^+\pi^-$ decays are considered: the first involving K^0_S mesons that decay early enough for the daughter pions to be reconstructed in the vertex detector; and the second consisting of K^0_S candidates that decay later such that track segments of the pions cannot be formed in the vertex detector. These categories are referred to as *long* and *downstream*, respectively. The long category has better mass, momentum and vertex resolution than the downstream category. Different types of charged hadrons are distinguished using information from two ring-imaging Cherenkov detectors. Photon, electron, and hadron candidates are identified by a calorimeter system consisting of scintillating-pad and preshower detectors, an electromagnetic calorimeter, and a hadronic calorimeter. Muons are identified by a system composed of alternating layers of iron and multiwire proportional chambers. The online event selection system (trigger) [5] consists of a hardware stage, based on information from the calorimeter and muon systems, followed by a software stage.

3. Concept of tree-level γ measurements

It is possible to measure γ relying only on tree-level Feynman diagrams. This is based on the interference between $b \to c$ and $b \to u$ transitions, of which one such process is the decay $B^\pm \to DK^\pm$. As can be seen in Fig. 1, the daughter D meson can be both a D^0 and a $\overline{D}^0$ meson.

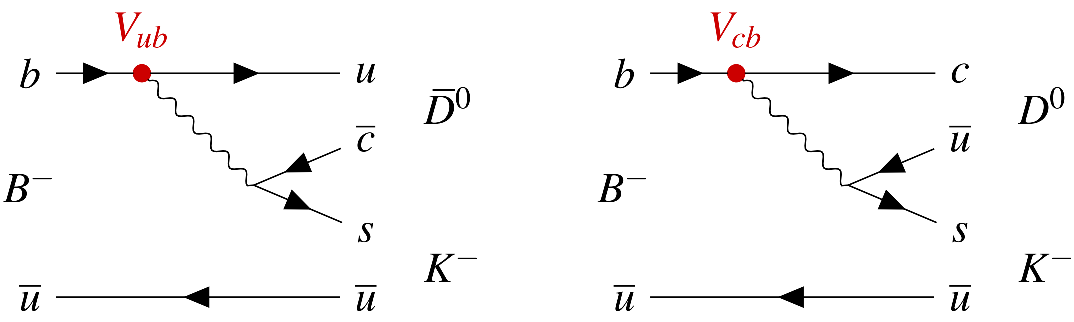

Figure 1: Feynman diagrams for $B^{\pm} \to DK^{\pm}$ decays.

The two decay amplitudes $A(B^- \to D^0K^-)$ and $A(B^- \to \bar{D}^0K^-)$ differ by a factor $r_B e^{i(\delta_B - \gamma)}$, where r_B is the magnitude of the ratio of the decay amplitudes, and δ_B a strong phase difference. The sensitivity on γ depends on the size of r_B, as it represents the amount of interference. When changing the flavour of the decaying B meson, γ enters the equations with the opposite sign. Instead of directly fitting for γ the parametrizations

$$
\begin{aligned}
x_{\pm} &= r_B \cos(\delta_B \pm \gamma) \\
y_{\pm} &= r_B \sin(\delta_B \pm \gamma)
\end{aligned}
\tag{3.1}
$$

are often used, as they are more robust, especially when the statistics is small or the results are close to physics boundaries. The subsequent D decay can contain amplitude and phase differences as well, which requires input from charm decays. Depending on the D final state three methods are distinguished: in the `ADS` method [6] *CP* eigenstates like $D \to K\pi$ are used, in the `GLW` method [7,8] *CP*-even D decays like $D \to K^+K^-$ or $D \to \pi^+\pi^-$, and in the `GGSZ` method [9] multi-body D decays, which require the analysis of the corresponding Dalitz plot.

4. Measurement of the CKM angle γ using $B^0 \to DK^{*0}$ [10,11]

In the measurement of γ from studies of $B^0 \to DK^{*0}$ decays the flavour of the decaying B meson can be inferred from the charges of the decay products of the K^{*0} meson, as the decay of the K^{*0} is flavour specific. The D meson can be reconstructed in the $D \to K^0_S\pi^+\pi^-$ final state. This requires an analysis of the Dalitz plot of the D phase space. The amplitude of the D^0 and the $\bar{D}^0$ decay can be assumed to be the same but there is a strong phase difference δ_D between the two decay amplitudes, which differs throughout the phase space. The strong phase can either be described by a specific amplitude model [10] or the results of a measurement of δ_D in bins of the Dalitz plot can be used [11].

Model-dependent approach [10]

Certain mass window requirements on the K^0_S, K^{*0} and D candidates are applied. A boosted decision tree (BDT) [12,13] is trained to improve the signal purity. To disentangle signal from background a fit to the invariant DK^* mass is performed. Apart from the signal, which is parametrized with the sum of two Crystal Ball functions [14], components for $B^0_s \to DK^{*0}$ decays, combinatorial background, partially reconstructed $B^0_{(s)} \to D^* \overset{(-)}{K}{}^{*0}$ decays, and misidentified $B^0 \to D\rho^0$ decays, are included in the fit model (see Fig. 2). The mass fit yields 89 ± 11 $B^0 \to DK^{*0}$ candidates in a $\pm 25\,\mathrm{MeV}/c^2$ mass window around the B^0 mass. In this mass window the *CP* fit is performed.

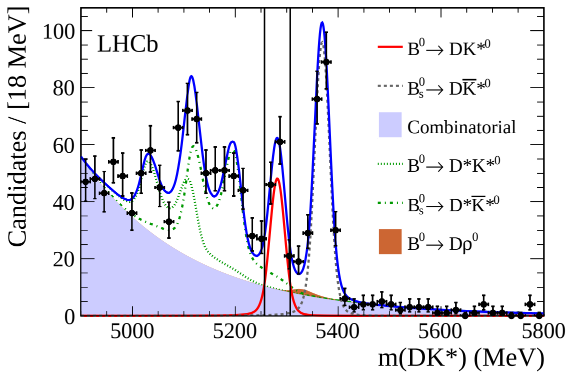

Figure 2: Invariant mass distribution for $B^0 \to DK^{*0}$ long and downstream candidates.

The efficiencies in the Dalitz plot are determined using simulations. The decay rates of B^0 and $\bar{B}^0$ can be expressed as

$$\begin{aligned} d\Gamma(B^0 \to DK^{*0}) &\propto |A_D|^2 + r_{B^0}^2 |\overline{A}_D|^2 + 2\,\kappa \mathrm{Re}\left(A_D^* \overline{A}_D (x_+ + \mathrm{i}\, y_+)\right) , \\ d\Gamma(\bar{B}^0 \to D\bar{K}^{*0}) &\propto |A_D|^2 + r_{B^0}^2 |\overline{A}_D|^2 + 2\,\kappa \mathrm{Re}\left(A_D^* \overline{A}_D (x_- + \mathrm{i}\, y_-)\right) , \end{aligned} \tag{4.1}$$

where the amplitude model developed by BaBar [15] is applied for A_D and $\overline{A}_D$ and the coherence factor κ is taken from the $B^0 \to DK^+\pi^-$ amplitude analysis [16]. The *CP* parameters are measured to be

$$\begin{aligned} x_+ &= 0.05 \pm 0.24 \pm 0.04 \pm 0.01 , \\ x_- &= -0.15 \pm 0.14 \pm 0.03 \pm 0.01 , \\ y_+ &= -0.65\,{}^{+0.24}_{-0.23} \pm 0.08 \pm 0.01 , \\ y_- &= 0.25 \pm 0.15 \pm 0.06 \pm 0.01 , \end{aligned}$$

where the first uncertainty is statistical, the second systematic and the third covers the uncertainties introduced by the specific amplitude model, which are currently negligible compared to the other uncertainties. The largest systematic uncertainties arise from the invariant mass fit and the description of non-D background contributions. The values for $x_\pm$ and $y_\pm$ are transferred to

$$\gamma = \left(80^{+21}_{-22}\right)^\circ , \quad r_B = 0.39 \pm 0.13 , \quad \delta_B = \left(197^{+24}_{-20}\right)^\circ .$$

Model-independent approach [11]

In the model-independent approach a very similar selection strategy is applied consisting of a rather loose preselection followed by a boosted decision tree and some particle identification requirements. The statistics is increased by reconstructing as well $D \to K^0_S K^+ K^-$ decays. A simultaneous fit to the invariant mass distribution of both final states is performed in the range

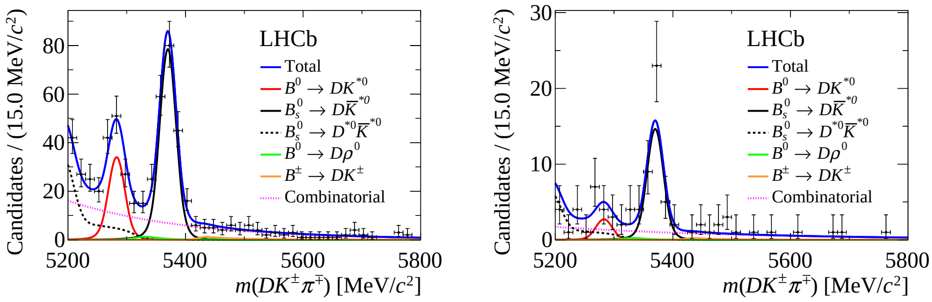

Figure 3: Invariant mass distributions of $B^0 \to DK^{*0}$ candidates with (left) $D \to K_S^0\pi^+\pi^-$ and (right) $D \to K_S^0K^+K^-$. The fit results, including the signal and background components, are superimposed.

$5200–5800\,\mathrm{MeV}/c^2$. The lower mass boundary is higher than in the previously described model-dependent approach, which allows to neglect a component for $B^0 \to D^{*0}K^{*0}$ decays. All other components are the same as before. The resulting mass distributions are shown in Fig. 3.

The Dalitz plot shown in Fig. 4 is symmetrically binned into two times eight and two times two bins for the $D \to K_S^0\pi^+\pi^-$ and $D \to K_S^0K^+K^-$ final states, respectively. The expected number of candidates in bin i is given by

$$N_i(B^0) = n_{B^0}\left[F_{-i} + (x_+^2 + y_+^2)F_i + 2\kappa\sqrt{F_iF_{-i}}(x_+c_i - y_+s_i)\right],$$
$$N_i(\bar{B}^0) = n_{\bar{B}^0}\left[F_i + (x_-^2 + y_-^2)F_{-i} + 2\kappa\sqrt{F_iF_{-i}}(x_-c_i + y_-s_i)\right],$$

where F_i, the efficiency-corrected fraction of $D \to K_S^0h^+h^-$ candidates in bin i, is determined using $B^0 \to D^{*-}\mu^+\nu_\mu$ decays with $D^{*-} \to \bar{D}^0\pi^-$, and the values for $c_i = \cos\delta_D(i)$ and $s_i = \sin\delta_D(i)$ are taken from a CLEO measurement using quantum-correlated $\psi(3770) \to D^0\bar{D}^0$ decays [17].

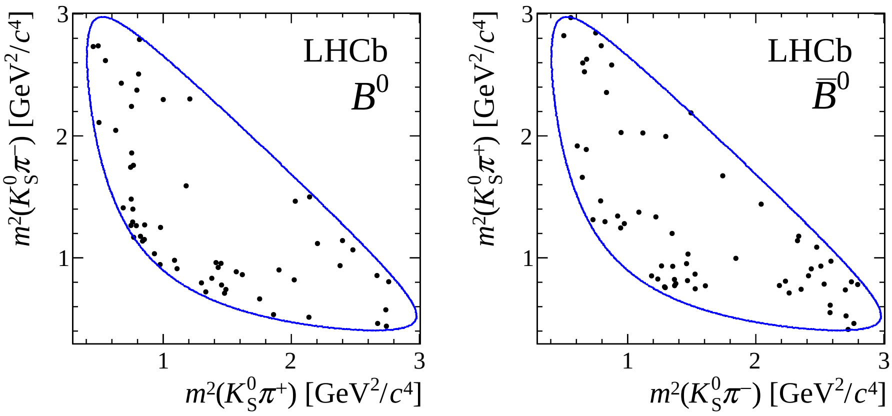

Figure 4: Dalitz plots of candidates in the signal region for $D \to K_S^0\pi^+\pi^-$ decays from (left) $B^0 \to DK^{*0}$ and (right) $\bar{B}^0 \to D\bar{K}^{*0}$ decays. The solid blue line indicates the kinematic boundary.

The results of the *CP* parameters

$$\begin{aligned} x_+ &= 0.05 \pm 0.35(\text{stat}) \pm 0.02(\text{syst})\,, \\ x_- &= -0.31 \pm 0.20(\text{stat}) \pm 0.04(\text{syst})\,, \\ y_+ &= -0.81 \pm 0.28(\text{stat}) \pm 0.06(\text{syst})\,, \\ y_- &= 0.31 \pm 0.21(\text{stat}) \pm 0.05(\text{syst})\,, \end{aligned}$$

are very similar to the ones of the model-dependent approach but slightly less precise. The latter changes when translating the values to γ because a higher value for r_B is measured:

$$\gamma = (71 \pm 20)^\circ\,, \quad r_B = 0.56 \pm 0.17\,, \quad \delta_B = \left(204^{+21}_{-20}\right)^\circ\,.$$

A direct comparison between the model-dependent and the model-independent approach is given in Fig. 5, where the x-y-plane is depicted.

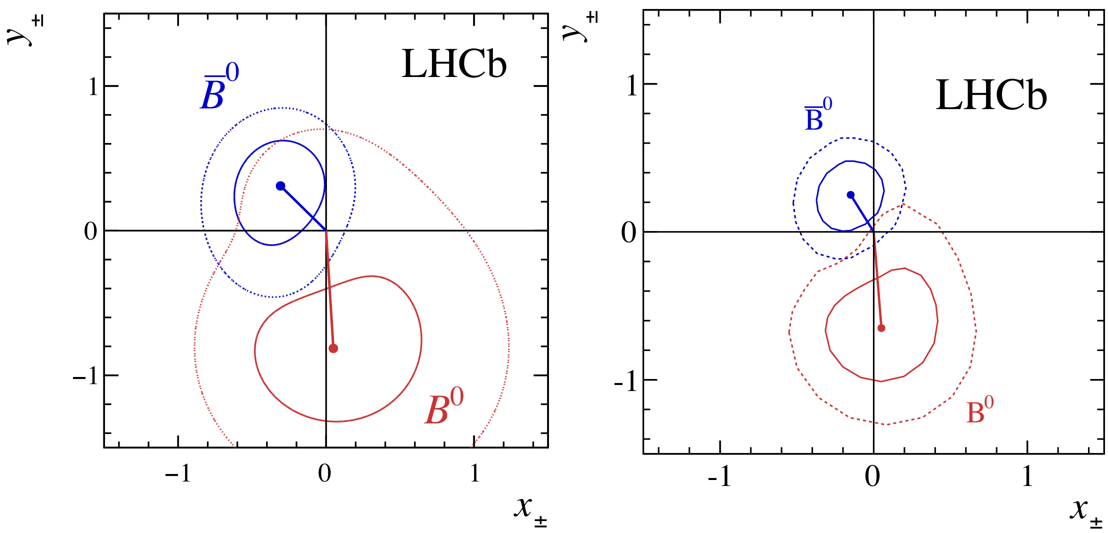

Figure 5: Confidence levels at (solid) 68.3 % and (dotted) 95.5 % for (red, light) (x_+, y_+) and (blue, dark) (x_-, y_-) as measured in $B^0 \to DK^{*0}$ decays (statistical uncertainties only) for (left) the model-independent analysis [11] and (right) the model-dependent approach [10]. The points represent the best fit values.

5. Constraints on the unitarity triangle angle γ from Dalitz plot analysis of $B^0 \to DK^+\pi^-$ decays [16]

Candidate $B^0 \to DK^+\pi^-$ decays are selected with the D meson decaying into the $K^+\pi^-$, K^+K^- or $\pi^+\pi^-$ final state. After some loose requirements and vetoes to remove exclusive backgrounds, neural networks (NNs), one for each D decay mode, are trained to separate the signal from the remaining background. The networks make use of input variables that describe the corresponding decay topology. Loose requirements are applied on the NNs. The resulting samples are divided into five bins, which have a similar number of signal decays. A simultaneous mass fit is performed

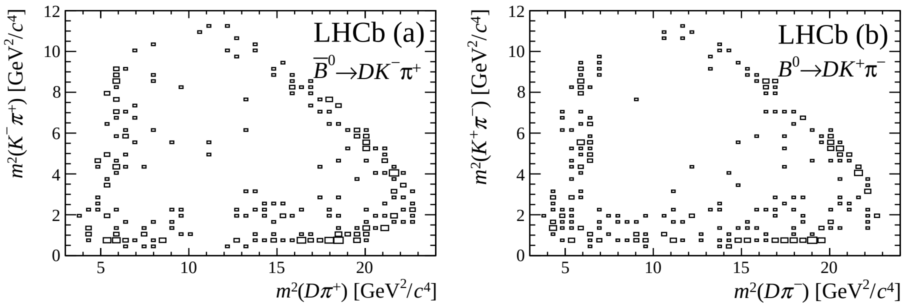

Figure 6: Dalitz plots for candidates in the B candidate mass signal region in the $D \to K^+K^-$ and $D \to \pi^+\pi^-$ samples for (a) $\bar{B}^0$ and (b) B^0 candidates. Background has not been subtracted, and therefore some contribution from $\bar{B}^0_s \to D^{*0}K^+\pi^-$ decays is expected at low $m(DK^+)$ (*i.e.* along the top right diagonal).

in the five bins and the results are statistically combined. For the analysis of the Dalitz plot, which is shown in Fig. 6, only the candidates in the 2.5σ window around the B^0 peak are used. The decay amplitude is parametrized with the isobar model:

$$A\left(m^2(D\pi^-), m^2(K^+\pi^-)\right) = \sum_{j=1}^{N} c_j F_j \left(m^2(D\pi^-), m^2(K^+\pi^-)\right).$$

The functions F_j describe the resonant dynamics considering line shape, angular distributions and barrier factors as a function of the phase space $\left(m^2(D\pi^-), m^2(K^+\pi^-)\right)$. The parametrization of the $D\pi$ system takes into account contributions from $D_0^*(2400)^-$, $D_2^*(2460)^-$, and $D\pi^-$ S- and P-waves. The masses and widths of the resonances in the $D\pi$ system are constrained. In the $K\pi$ system the masses and widths of the resonances $K^*(892)^0$, $K^*(1410)^0$, and $K_2^*(1430)^0$ are fixed. Additionally, a $K^+\pi^-$ S-wave component is considered. Only for the complex coefficient c_j of the $K^*(892)^0$ contribution *CP* violation is allowed in the fit. The fit results for $x_\pm$ and $y_\pm$ show no significant *CP* violation. Neither a non-zero value for r_B can be established nor any value for γ can be excluded at 95 % confidence level.

6. Measurement of *CP* observables in $B^\pm \to DK^\pm$ and $B^\pm \to D\pi^\pm$ with two- and four-body D decays [18]

When reconstructing the D mesons of $B^\pm \to Dh^\pm$ decays ($h = K^\pm$ or $\pi^\pm$) in the $K^+\pi^-$ or in the $K^+\pi^-\pi^+\pi^-$ final state, large interference between the $B^- \to D^0h^-$ and the $B^- \to \bar{D}^0h^-$ decay rates occurs. The reason is that both amplitudes are the combination of a Cabibbo-favoured and a Cabibbo-suppressed decay (ADS method). The decay rate is given by

$$\Gamma(B^\pm \to f_D h^\pm) \propto (r_D^f)^2 + r_B^2 + 2\, r_B\, r_D^f\, \kappa_D^f \cos(\delta_B + \delta_D^f \pm \gamma)\,, \tag{6.1}$$

where r_D^f and r_B are the ratio of the suppressed and favoured amplitudes of the D and B decays, respectively. For the two-body final state the coherence factor κ_D^f is unity while for the four-body final state it has been measured to be $\kappa_D^{K3\pi} = 0.32^{+0.12}_{-0.08}$ [19]. One of the observables that are determined in this analysis is the charge asymmetry

$$A \equiv \frac{\Gamma(B^- \to f_D h^-) - \Gamma(B^+ \to \overline{f}_D h^+)}{\Gamma(B^- \to f_D h^-) + \Gamma(B^+ \to \overline{f}_D h^+)}, \tag{6.2}$$

which can be directly calculated from the efficiency-corrected B^- and B^+ yields. Although the samples with bachelor pions are clearly larger and thus have smaller statistical uncertainties than the ones with bachelor kaons, the most significant asymmetry, in fact even the first observation of *CP* violation with a single $B \to Dh$ mode, is achieved in $B \to DK$ with $D \to K\pi$:

$$A^{\pi K}_{\mathrm{ADS}(K)} = -0.403 \pm 0.056(\mathrm{stat}) \pm 0.011(\mathrm{syst})\,.$$

A fit to the invariant mass distributions of selected $B \to DK$ decays is shown in Fig. 7.

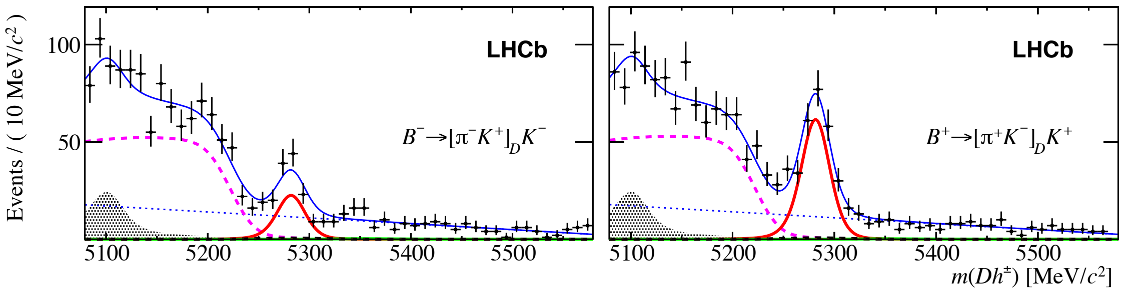

Figure 7: Invariant mass distributions of selected $B \to DK$ decays, separated by charge. The dashed pink line left of the signal peak (red, thick) shows partially reconstructed $B^0_s \to DK^-\pi^+$ decays, where the bachelor pion is missed.

Another approach is to reconstruct D final states that are *CP* eigenstates (GLW method). In this case, the decay rates simplify to

$$\Gamma(B^{\mp} \to f_D h^{\mp}) \propto 1 + r_B^2 + 2\,r_B\,(2F_+ - 1)\,\cos(\delta_B \mp \gamma)\,, \tag{6.3}$$

as r_D is unity and δ_D is zero. While the two-body final states $\pi^+\pi^-$ and K^+K^- are totally *CP*-even ($F_+ = 1$), the fraction of the *CP*-even component in the four-body D final state $\pi^+\pi^-\pi^+\pi^-$ is determined to be $F_+^{4\pi} = 0.737 \pm 0.028$ [20]. For the first time *CP* asymmetries with this four-body D final state are determined, among others the charge asymmetry:

$$A^{\pi\pi\pi\pi}_{\mathrm{GLW}(K)} = 0.100 \pm 0.034(\mathrm{stat}) \pm 0.018(\mathrm{syst})\,.$$

7. Measurement of the CKM angle γ from a combination of $B \to DK$ analyses [21]

The tree-level measurements of the CKM angle γ from $B \to DK$ decays are combined. The combination comprises results from $B^{\pm} \to DK^{\pm}$, $B^0 \to DK^{*0}$, $B^+ \to DK^+\pi^+\pi^-$, and $B^0_s \to D^{\mp}_s K^{\pm}$ decays and follows a frequentist treatment. To obtain the best precision, the hadronic parameters are also considered in the combination. The average value $\gamma = \left(70.9^{+7.1}_{-8.5}\right)^{\circ}$ is the most precise single-experiment measurement to date. The shapes of the $1-\mathrm{CL}$ curves, split by the method, are shown in Fig. 8.

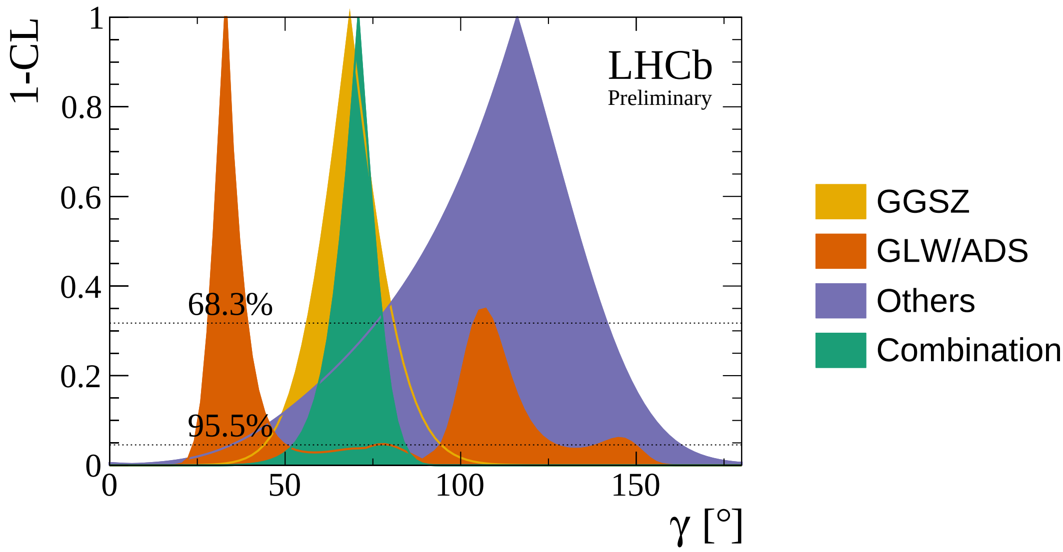

Figure 8: $1-\mathrm{CL}$ curves for the combination of the γ measurements and the contributions from the individual methods.

8. Conclusion

With the world's largest sample of B-hadrons LHCb has performed many promising measurements of γ. Using the GGSZ method $B^0 \to DK^{*0}$ decays have been analysed with a model-dependent and a model-independent approach. The ADS and the GLW method have been applied to measure the asymmetries in $B \to Dh$ decays using two- and four-body final states. All $B \to DK$ modes are combined into an average value of $\gamma = \left(70.9^{+7.1}_{-8.5}\right)^\circ$, which represents the most precise measurement from a single experiment. This result will even be improved once the $B \to D\pi$ modes are included as well.

References

[1] N. Cabibbo, *Unitary symmetry and leptonic decays*, Phys. Rev. Lett. **10** (1963) 531.

[2] M. Kobayashi and T. Maskawa, *CP violation in the renormalizable theory of weak interaction*, Prog. Theor. Phys. **49** (1973) 652.

[3] LHCb collaboration, A. A. Alves Jr. *et al.*, *The LHCb detector at the LHC*, JINST **3** (2008) S08005.

[4] LHCb collaboration, R. Aaij *et al.*, *LHCb detector performance*, Int. J. Mod. Phys. **A30** (2015) 1530022, arXiv:1412.6352.

[5] R. Aaij *et al.*, *The LHCb trigger and its performance in 2011*, JINST **8** (2013) P04022, arXiv:1211.3055.

[6] D. Atwood, I. Dunietz, and A. Soni, *Enhanced cp violation with* $B \to \mathrm{kd}^0(\overline{d}^0)$ *modes and extraction of the cabibbo-kobayashi-maskawa angle* γ, Phys. Rev. Lett. **78** (1997) 3257, arXiv:9612433.

[7] M. Gronau and D. London, *How to determine all the angles of the unitarity triangle from B(d)0 —> D K(s) and B(s)0 —> D0*, Phys. Lett. **B253** (1991) 483.

[8] M. Gronau and D. Wyler, *On determining a weak phase from CP asymmetries in charged B decays*, Phys. Lett. **B265** (1991) 172.

[9] A. Giri, Y. Grossman, A. Soffer, and J. Zupan, *Determining gamma using B+- —> DK+- with multibody D decays*, Phys. Rev. **D68** (2003) 054018, arXiv:hep-ph/0303187.

[10] LHCb collaboration, R. Aaij *et al.*, *Measurement of the CKM angle γ using $B^0 \to DK^{*0}$ with $D \to K^0_S \pi^+\pi^-$ decays*, arXiv:1605.01082, submitted to JHEP.

[11] LHCb collaboration, R. Aaij *et al.*, *Model-independent measurement of the CKM angle γ using $B^0 \to DK^{*0}$ decays with $D \to K^0_S \pi^+\pi^-$ and $K^0_S K^+K^-$*, arXiv:1604.01525, to appear in JHEP.

[12] L. Breiman, J. H. Friedman, R. A. Olshen, and C. J. Stone, *Classification and regression trees*, Wadsworth international group, Belmont, California, USA, 1984.

[13] B. P. Roe *et al.*, *Boosted decision trees as an alternative to artificial neural networks for particle identification*, Nucl. Instrum. Meth. **A543** (2005) 577, arXiv:physics/0408124.

[14] T. Skwarnicki, *A study of the radiative cascade transitions between the Upsilon-prime and Upsilon resonances*, PhD thesis, Institute of Nuclear Physics, Krakow, 1986, DESY-F31-86-02.

[15] BaBar, P. del Amo Sanchez *et al.*, *Evidence for direct CP violation in the measurement of the Cabibbo-Kobayashi-Maskawa angle gamma with B-+ —> D(*) K(*)-+ decays*, Phys. Rev. Lett. **105** (2010) 121801, arXiv:1005.1096.

[16] LHCb collaboration, R. Aaij *et al.*, *Constraints on the unitarity triangle angle γ from Dalitz plot analysis of $B^0 \to DK^+\pi^-$ decays*, arXiv:1602.03455, to appear in Phys. Rev. D.

[17] CLEO, J. Libby *et al.*, *Model-independent determination of the strong-phase difference between D^0 and $\bar{D}^0 \to K^0_{S,L} h^+h^-$ $(h = \pi, K)$ and its impact on the measurement of the CKM angle γ/ϕ_3*, Phys. Rev. **D82** (2010) 112006, arXiv:1010.2817.

[18] LHCb collaboration, R. Aaij *et al.*, *Measurement of CP observables in $B^\pm \to DK^\pm$ and $B^\pm \to D\pi^\pm$ with two- and four-body D meson decays*, arXiv:1603.08993, submitted to Phys. Lett. B.

[19] T. Evans *et al.*, *Improved determination of the $D \to K^-\pi^+\pi^+\pi^-$ coherence factor and associated hadronic parameters from a combination of $e^+e^- \to \psi(3770) \to c\bar{c}$ and $pp \to c\bar{c}X$ data*, Phys. Lett. **B757** (2016) 520, arXiv:1602.07430.

[20] S. Malde *et al.*, *First determination of the CP content of $D \to \pi^+\pi^-\pi^+\pi^-$ and updated determination of the CP contents of $D \to \pi^+\pi^-\pi^0$ and $D \to K^+K^-\pi^0$*, Phys. Lett. **B747** (2015) 9, arXiv:1504.05878.

[21] LHCb collaboration, *LHCb γ combination update from $B \to DK$ decays*, LHCb-CONF-2016-001.